

# Scaling Theory for the Frictionless Unjamming Transition

Kabir Ramola\* and Bulbul Chakraborty†

*Martin Fisher School of Physics, Brandeis University, Waltham, MA 02454, USA*

(Dated: November 18, 2018)

We develop a statistical framework for the unjamming transition of soft frictionless disks in two dimensions. We describe the system in terms of local areas ( $a$ ), which can be uniquely assigned to each contact. These microscopic degrees of freedom serve to define *local* order parameters, and allow us to probe the origin of the widely noted scaling of *global* physical properties near the unjamming transition. We find that the scaling with energy  $E_G$  near the transition can be attributed to divergences in the distributions of these local areas, which can be clearly separated into contributions arising from locally ordered structures and a disordered piece. We derive scaling forms for these divergences in each of these distributions. We show that the asymptotic behaviour of these scaling forms arises from the geometrical structure of the packing while the overall scaling with energy depends on the force law. We use these scaling forms to determine the scaling of the total grain area  $A = \sum a$ . For disks interacting via linear spring potentials, as the energy of the system approaches zero,  $E_G \rightarrow 0^+$ , and the number of contacts  $N_C$  approaches its isostatic value, we find  $\Delta A \sim \Delta N_C$  and  $\Delta A \sim E_G^{1/4}$ . We test our predictions using large scale simulations of bidispersed disks.

PACS numbers: 83.80.Fg, 81.05.Rm, 64.70.Q-, 61.43.-j, 61.20.-p, 45.70.-n

*Introduction:* The jamming of soft particles has been of continued interest in the field granular physics [1–9]. In addition, it is also used as a paradigm to study glassy systems [10–12], active matter [13] and biological tissues [14] amongst others. Frictionless soft disks and spheres serve as a first approximation to many theoretical models and have been extensively investigated over the last decade [15–27]. The unjamming transition of soft spheres exhibits properties reminiscent of critical points in equilibrium systems. Observations include power laws [16], a scaling form for the energy analogous to free energy and resulting relationships between scaling exponents [26], scaling collapse of dynamical quantities such as viscosity [28], and indications of diverging length scales [20]. Many scaling properties of soft particles near the jamming transition have been analysed in detail [29, 30], and finite-size scaling studies seem to suggest a mixed order transition with two critical exponents [18, 20]. However, despite considerable effort towards a unifying theory, a clear description is still lacking, and the origin of various power laws in this system have remained somewhat mysterious. Theories so far have focussed on the behavior of global quantities such as energy, packing fraction, pressure, stresses, and the total contact numbers. This is in contrast to the norm in studying critical points where a local order parameter and its distribution within the system is of primary importance.

In this letter we highlight how the underlying disorder in jammed systems naturally leads to diverging contributions to distributions of local quantities. This in turn leads to non-trivial power laws involving global quantities such as the excess contact number, and the areas occupied by grains. Our treatment relies on local grain areas assigned to individual contacts that play the role of “quasiparticles”. We use the underlying distribution of interparticle distances and angles to derive a density of

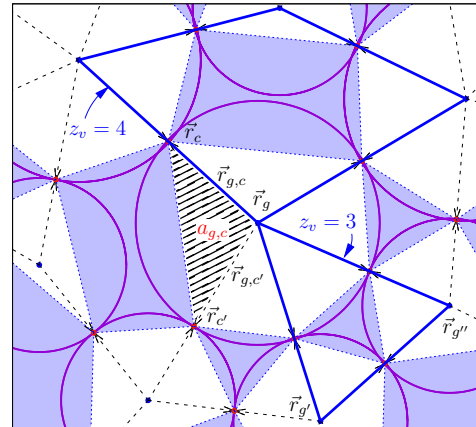


FIG. 1: A section of a jammed configuration of soft frictionless disks. The centers of the grains with radii  $\{\sigma_g\}$  are located at positions  $\{\vec{r}_g\}$ . The contact points between grains are located at positions  $\{\vec{r}_c\}$ , with contact vectors  $\vec{r}_{g,c} = \vec{r}_c - \vec{r}_g$ . The distance vectors  $\vec{r}_{g,g'} = \vec{r}_{g'} - \vec{r}_g$  form a network of faces (minimum cycles) with  $z_v$  sides each. The polygonal tiling associated with the packing partitions the space into areas occupied by grains (white) and areas occupied by voids (blue). The triangle formed by the points  $(\vec{r}_g, \vec{r}_c, \vec{r}_{c'})$  (shaded area) is uniquely assigned to the contact  $c$  and has an associated area  $a \equiv a_{g,c}$ , with a normalized area  $\alpha_c = a_{g,c}/\sigma_g^2$ .

states of these triangular units. As will be clear from our analysis, the need for using triangular units as the basic objects in describing the scaling behavior highlights the importance of *three-body interactions* as opposed to two-body terms such as interparticle distances that had been considered in the literature. We focus specifically on the unjamming transition of soft disks, i.e. we approach the transition point from mechanically stable (jammed) packings with decreasing energies ( $E_G \rightarrow 0^+$ ). In such

jammed states, the disks organize into complicated “random” structures which are hard to characterise owing to the complexity of the non-convex curved shapes formed by voids. In order to avoid this problem we construct polygonal tilings that partitions space into areas occupied by grains and areas occupied by the voids (see Fig. 1). This construction serves to define a reliable local order parameter with which to describe the unjamming transition [27], and bears similarities to the “quadron” framework [32–34]. We assign these polygonal areas uniquely to the contacts with an associated area  $\alpha$  (normalized by the size of the disks). We show that the density of states of these local areas can be expressed as

$$p(\alpha) = \underbrace{p_{\text{reg}}(\alpha) + p_{\text{DO}}(\alpha)}_{p(\alpha, >3)} + \underbrace{p_{\text{O}}(\alpha)}_{p(\alpha, 3)}, \quad (1)$$

where  $p_{\text{DO}}$  and  $p_{\text{O}}$  are classified as “disordered” and “ordered” divergences respectively. In our definition disordered structures are voids formed by four or more disks in contact (labelled as  $> 3$ ), and ordered structures arise from voids formed by three disks (labelled with 3). Each of these divergent terms can be written in terms of a scaling form. The main result of this letter is the derivation of a scaling form for  $p_{\text{DO}}$ , which we then use to derive scaling properties of global quantities. For simplicity we present results for monodispersed disks, the generalization to the polydispersed case is straightforward, and will be discussed in the context of our numerical simulations. For the disordered divergence, we find

$$p_{\text{DO}}(\alpha) = E_G^{-1/4} \mathcal{P}_{\text{DO}} \left( \frac{\frac{1}{2} - \alpha}{\sqrt{E_G}} \right) \quad (2)$$

which possesses the following asymptotic behaviour

$$\mathcal{P}_{\text{DO}}(x) \sim \begin{cases} x^{3/2}, & x \rightarrow 0, \\ x^{-1/2}, & x \rightarrow \infty. \end{cases} \quad (3)$$

Similarly we find that the “ordered” distribution has a scaling form

$$p_{\text{O}}(\alpha) = E_G^{-1/2} \mathcal{P}_{\text{O}} \left( \frac{\frac{\sqrt{3}}{4} - \alpha}{\sqrt{E_G}} \right), \quad (4)$$

which is integrable in the  $E_G \rightarrow 0^+$  limit. As the system approaches the unjamming transition, the total number of contacts ( $N_C$ ) decreases and attains its isostatic value  $N_C(0) = 4N_G - 2$ . The abovementioned scaling behaviour leads to the following relation for the excess number of contacts  $\Delta N_C = N_C(E_G) - N_C(0)$  with energy

$$\Delta N_C \sim E_G^{1/4}, \quad (5)$$

that has been observed in several studies [16, 26, 27, 31].

*Energy Ensemble and Local Areas:* We begin our analysis by considering the fixed energy ensemble [27] for a system of jammed soft disks in two dimensions. The volume of the total space is kept fixed with linear dimensions  $L_x = L_y = 1$ . We consider all possible grain positions  $\{\vec{r}_g\}$  and radii  $\{\sigma_g\}$  that yield a force balanced jammed state. The disks interact via a linear spring potential of the interparticle distances  $\vec{r}_{g,g'} = \vec{r}_{g'} - \vec{r}_g$  of the form

$$V[\{\vec{r}_g, \sigma_g\}] = \sum_{g \neq g'} \frac{1}{2} \left( 1 - \frac{|\vec{r}_{g,g'}|}{\sigma_{g,g'}} \right)^2 \Theta \left( 1 - \frac{|\vec{r}_{g,g'}|}{\sigma_{g,g'}} \right), \quad (6)$$

with  $\sigma_{g,g'} = \sigma_g + \sigma_{g'}$ . We then consider the ensemble of all jammed (force-balanced) configurations at a fixed energy  $E_G = \sum_g V[\{\vec{r}_g, \sigma_g\}]$ .

A jammed state of frictionless disks is characterised by a system spanning contact network which naturally partitions the space into convex minimum cycles (or faces) of  $z_v$  sides each (see Fig. 1). The system can then be parametrized in terms of the interparticle distance vectors  $\{\vec{r}_{g,g'}^i\}$  where the index  $i$  labels the vectors within each cycle. The loop constraints around each face account for the overcounting of the degrees of freedom and can be implemented as

$$\{\vec{r}_g\} \rightarrow \{\vec{r}_{g,g'}\} \times \prod_v \delta \left( \sum_{i=1}^{z_v} \vec{r}_{g,g'}^i \right). \quad (7)$$

As we show, these constraints provide the correlations that are crucial in determining the internal structures and in turn the scaling behaviour near the transition. We next use the contact points to assign areas to individual contacts. The positions of the contacts are represented by the set of contact points  $\{\vec{r}_c\}$  with  $\vec{r}_c = \vec{r}_g + \frac{\sigma_g}{\sigma_g + \sigma_{g'}} (\vec{r}_{g'} - \vec{r}_g)$ , where  $c$  is the contact between grains  $g$  and  $g'$ , and contact vectors  $\vec{r}_{g,c} = \vec{r}_c - \vec{r}_g$ . Each contact is counted twice, once for each grain (see Fig. 1). Following the network representation introduced in [27], we define local and global order parameters as

$$a_{g,c} = \frac{1}{2} (\vec{r}_{g,c} \times \vec{r}_{g,c'}) \quad \text{and} \quad A_G = \sum_{c=1}^{N_C} a_{g,c}.$$

where  $\vec{r}_{g,c}$  and  $\vec{r}_{g,c'}$  are adjacent contact vectors (see Fig. 1) and the convention is that the area bounded by  $(c, c')$  is uniquely assigned to the contact  $c$ . The individual contact areas play the role of a local packing fraction in our description. These individual areas  $a_{g,c}$  can vary between 0 and  $\frac{1}{2}\sigma_g^2$  where  $\sigma_g$  is the radius of the grain to which they belong. In order to account for the varying sizes of the grains between configurations at a fixed global energy, we work with the following normalized area  $\alpha_c = a_{g,c}/\sigma_g^2$ , which is bounded between  $[0, \frac{1}{2}]$ . Similarly we normalize the contact vectors by the size of the disks, with  $|\vec{r}_{g,c}| \rightarrow |\vec{r}_{g,c}|/\sigma_g$  now being bounded between  $[0, 1]$ .

*Distribution of areas:* To proceed we assume that the underlying system is *disordered*, and has reproducible local distributions. The distribution of contact vector lengths can be directly related to the total energy of the system (from Eq. 6). We can then use this underlying distribution to derive an expression for the distribution of areas  $p(\alpha)$ . In a disordered jammed state, the overlaps between disks are fluctuating quantities  $\Delta r_{g,c}$  with  $|\vec{r}_{g,c}| = 1 - \Delta r_{g,c}$  and  $E_G = \frac{1}{N_G} \sum_{i=1}^{N_G} (\Delta r_{g,c})^2$ , which naturally leads to the following scaling form for the distribution of overlaps

$$p(\Delta r_{g,c}) = \frac{1}{\sqrt{E_G}} \mathcal{P}_r \left( \frac{\Delta r_{g,c}}{\sqrt{E_G}} \right). \quad (8)$$

The square-root scaling is specific to linear spring potentials, and reproduces the well-known force distribution curve. Changing the force law would change the exponent of  $E_G$ . Although the contact vectors,  $\vec{r}_{g,c}$ , have a complicated joint density, we focus on the two vectors  $\vec{r}_1, \vec{r}_2$  bounding a given area  $\alpha$ . We define  $p(\vec{r}_1, \vec{r}_2)$  as the joint probability of occurrence of contact vectors  $\vec{r}_1, \vec{r}_2$  at two contiguous edges of a minimum cycle. The probability of each individual area is then

$$p(\alpha) = \int d\vec{r}_1 \int d\vec{r}_2 p(\vec{r}_1, \vec{r}_2) \delta \left( \frac{1}{2} |\vec{r}_1| |\vec{r}_2| \sin \theta - \alpha \right), \quad (9)$$

where  $\theta$  is the relative angle between the two vectors. If the lengths of the contact vectors are held fixed, the vanishing slope of the sin function leads to a singularity in  $p(\alpha)$  at  $\theta = \pi/2$ . As the unjamming transition is approached, the fluctuations in the lengths decrease (Eq. (8)), leading to a sharpening divergence as the transition is approached, and indeed as we show, leads to the observed power-law scaling. In the disordered jammed state, we can justifiably assume that the distribution of contact vectors is independent of its orientation with  $p(\vec{r}_1) = \int d^2 \vec{r}_2 p(\vec{r}_1, \vec{r}_2) = \frac{1}{2\pi} p(|\vec{r}_1|)$ . The joint distribution of the two underlying contact vectors can then be expressed as

$$p(\vec{r}_1, \vec{r}_2) = p(|\vec{r}_1|) p(|\vec{r}_2|) p(\theta). \quad (10)$$

In the above decomposition, we have extracted the overall scaling with energy into the first two terms involving the magnitudes and the correlations are encoded in the function  $p(\theta)$ . We can develop a systematic diagrammatic expansion for the function  $p(\theta)$  (see Supplemental material). We find that the joint density  $p(\vec{r}_1, \vec{r}_2)$ , and consequently the areas can be classified into two categories:  $z_v > 3$  (disordered) corresponding to voids formed by four or more disks and  $z_v = 3$  (ordered) formed by three disks in contact. We use this classification to split the distribution as

$$p(\alpha) = \frac{g(\alpha)}{N_C} = p(\alpha, 3) + p(\alpha, > 3), \quad (11)$$

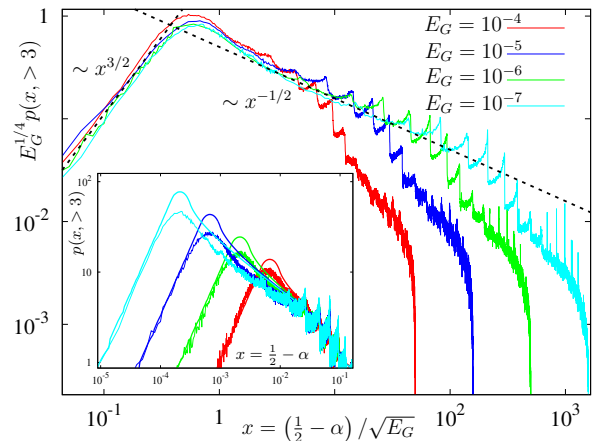


FIG. 2: Scaling collapse of the distribution of areas of the disordered cycles ( $z_v > 3$ ). The plot shows the distribution of  $x = (\frac{1}{2} - \alpha)$  for  $N_G = 4096$  disks.  $x \rightarrow 0$  corresponds to disks with contact angles close to  $\pi/2$ . The scaling is consistent with Eq. (2). The limiting behaviours of the distribution are provided in Eq. (3). **(Inset)** Comparison between the distributions obtained from the theory (bold lines) and numerical simulations. We find very good agreement between the two distributions, indicating that the theoretical analysis is able to capture the scaling with energy near the transition.

where  $g(\alpha)$  represents the density of states of normalized areas, with the normalization

$$\int_0^{1/2} p(\alpha, \geq 3) d\alpha = n_{\geq 3} / N_C, \quad (12)$$

where  $n_3$  and  $n_{>3}$  are the number of contact in cycles with 3 and  $> 3$  sides respectively, and  $n_3 + n_{>3} = N_C$ . As shown in the Supplemental material, the distribution of angles for the three disk structures are centered around a finite value  $\theta = \arcsin \frac{\sqrt{3}}{2}$ . This leads to an integrable divergence in the limit  $E_G \rightarrow 0^+$  in the distribution of areas from Eq. (9), and the scaling form can be shown to be as announced in Eq. (4). The contribution from these ordered structures to the disordered divergence at  $\theta = \pi/2$  is therefore exponentially suppressed. For the  $> 3$  case there is a finite contribution from  $\theta = \pi/2$ . To quantify the disordered divergence, we split the distribution into a divergent part arising from angles close to  $\pi/2$ , and a regular part that arises from the rest of the angular distribution

$$p(\alpha, > 3) = p_{\text{reg}}(\alpha) + p_{\text{DO}}(\alpha) \quad (13)$$

Without loss of generality, we assume that the angular distribution near  $\theta = \pi/2$  can be represented as a uniform distribution,  $p_{\pi/2}$  in the range  $[\frac{\pi}{2} - \Delta, \frac{\pi}{2} + \Delta]$ . This leads to the normalization for the regular part

$$\int_0^{1/2} p_{\text{reg}}(\alpha) d\alpha = p(\alpha, > 3) - 2\Delta p_{\pi/2}, \quad (14)$$

where the only energy dependence arises from the width  $\Delta$ . Making the change of variables  $\{\theta \rightarrow \sin \theta\}$  we have

$$p_{\text{DO}}(\sin \theta, > 3) = p_{\pi/2} (1 - \sin^2 \theta)^{-1/2} \quad \left| \theta - \frac{\pi}{2} \right| < \Delta. \quad (15)$$

Using this expression in Eq. (9) and performing the integration over  $\sin \theta$  we arrive at the following expression for the disordered divergence

$$p_{\text{DO}}(\alpha) = p_{\pi/2} \int_0^1 dr_1 \int_0^1 dr_2 \frac{p(r_1)p(r_2)}{\sqrt{r_1^2 r_2^2 - 4\alpha^2}} G(r_1, r_2, \alpha), \quad (16)$$

where  $G(r_1, r_2, \alpha)$  is a product of theta functions that ensures  $\sin(\frac{\pi}{2} - \Delta) < \frac{2\alpha}{r_1 r_2} < 1$ . The above expression has a singularity as  $\alpha \rightarrow 1/2$  and as  $r_1 \rightarrow 1$  and  $r_2 \rightarrow 1$ . Although the integral in Eq. (16) does not have a simple closed form answer for general  $p(r)$ , it is straightforward to extract its different limiting behaviours. In order to simplify the analysis further, we replace the distribution of the contact vectors in Eq. (8) with a uniform distribution. With this simplification, the integral can then be performed exactly (see Supplemental Material) and we find it obeys the scaling form announced in Eq. (3). From this analysis, it is evident that the asymptotic form of the scaling function in Eq. (3), the exponents  $1/2$  and  $3/2$ , arise from the purely geometric nature of the divergence at  $\theta \simeq \pi/2$ , whereas the square-root scaling with  $E_G$  is a consequence of the scaling of the distribution of contact lengths and is controlled by the force law.

*Numerical Simulations:* In order to test the predictions made by our theory, we perform large scale numerical simulations. Configurations are produced using a variant of the O'Hern protocol [16]. We simulate bidispersed systems with diameter ratio 1 : 1.4. The energies simulated range from  $E_G = 10^{-15}$  to  $10^{-3}$ , with the number of disks upto  $N_G = 8192$ . A scaling collapse of the distributions according to the scaling form in Eq. (2) is illustrated in Fig. 2. The two limiting behaviours announced in Eq. (3) are also illustrated. In the inset of Fig. 2 we show the distributions obtained from the theory along with the remarkable agreement with the distributions obtained from numerical simulations.

*Scaling Behaviour of Global Quantities:* The height of the peak of  $p_{\text{DO}}(\alpha)$  scales as  $E_G^{-1/4}$ , while the width scales as  $E_G^{1/2}$ . Since there are no discontinuities in the overall distribution, we can match the two parts of the distribution in Eq. (13) at a value  $\alpha^* = \frac{\Delta}{\sqrt{E_G}}$ . Since  $p_{\text{DO}}(\alpha^*) \sim E_G^{-1/4} \Delta$  and the regular part is independent of the energy, this provides the characteristic scale:

$$\lim_{E_G \rightarrow 0^+} \Delta E_G^{-1/4} = \text{Const.} \quad (17)$$

We can next use the scaling with  $E_G$  of the areas to derive global scaling properties of the system as the unjamming transition is approached. Since the microscopic areas are uniquely assigned to a contact, the incremental

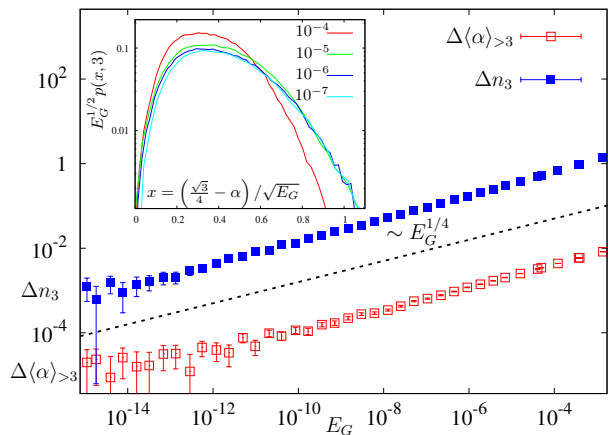


FIG. 3: Scaling of global quantities with energy as the unjamming transition is approached (i) the excess number of contacts in the ordered cycles ( $\Delta n_3 = n_3(E_G) - n_3(0)$ ) (ii) the excess normalized area per contact of the disordered cycles ( $\Delta \langle \alpha \rangle_{>3} = \langle \alpha \rangle_{>3}(E_G) - \langle \alpha \rangle_{>3}(0)$ ). The scaling is consistent with the predictions in Eqs. (19) and (20) (**Inset**) Scaling collapse of the distribution of areas of the ordered cycles  $p(\alpha, 3)$  around the divergence at  $\alpha = \sqrt{3}/4$ . The plot shows the distribution of  $x = \left(\frac{\sqrt{3}}{4} - \alpha\right) / \sqrt{E_G}$  for  $N_G = 4096$  disks at different energies. The scaling is consistent with Eq. (4).

global area covered by grains,  $\Delta A(E_G) = A(E_G) - A(0)$  has to scale as the excess number of contacts. We, therefore focus on how the excess number of contacts scale with  $E_G$ . Since the regular part of the density of states,  $g(\alpha)$  (Eq. (11)), is independent of energy, however,  $p_{\text{reg}}$  has an energy dependence from Eqs. ((13),(14) and (17), the number of contacts acquires a scaling with  $E_G$ :

$$N_C = \frac{\int_0^{1/2} g_{\text{reg}}(\alpha) d\alpha}{\int_0^{1/2} p_{\text{reg}}(\alpha) d\alpha} = N_C(0) + N_{C,1/4} E_G^{1/4} + \dots \quad (18)$$

which is the scaling relation mentioned in Eq. (5). Two *new* predictions follow immediately from this analysis: The excess number of contacts in the different cycles ( $\Delta n_{\geq 3} = n_{\geq 3}(E_G) - n_{\geq 3}(0)$ ) scale as

$$\Delta n_3 \sim E_G^{1/4}; \quad \Delta n_{>3} \sim \mathcal{O}(E_G^{1/2}), \quad (19)$$

while the excess normalized areas per contact ( $\Delta \langle \alpha \rangle_{\geq 3} = \langle \alpha \rangle_{\geq 3}(E_G) - \langle \alpha \rangle_{\geq 3}(0)$ ) scale as

$$\Delta \langle \alpha \rangle_3 \sim \mathcal{O}(E_G^{1/2}); \quad \Delta \langle \alpha \rangle_{>3} \sim E_G^{1/4}. \quad (20)$$

This behaviour is illustrated in Fig. 3.

*Discussion:* We derived the scaling behaviour for the unjamming transition of frictionless soft disks based on the local units of areas associated with contacts. We found that a simple analysis using the underlying distribution of contact vector lengths reproduces several properties of jammed systems remarkably well. The primary

scaling in the system arises from contact vectors with relative angles close  $\pi/2$ , which in the area representation have the highest susceptibilities to changes in energy. These structures therefore contribute overwhelmingly to the scaling at low energies. In this letter we have focussed on the distributions of individual areas, which involved a three-body interaction between disks. The contributions from the correlations between these individual units is non-trivial, and indeed leads to corrections from the simple exponents derived in this letter [27]. It would be interesting to see what role such long range correlations play in jammed systems close to the unjamming transition.

*Acknowledgements:* This work has been supported by NSF-DMR 1409093 and the W. M. Keck Foundation.

---

\* Electronic address: kramola@brandeis.edu

† Electronic address: bulbul@brandeis.edu

- [1] M. van Hecke, J. Phys.: Condens. Matter **22**, 033101 (2010).
- [2] A. J. Liu and S. R. Nagel, Annu. Rev. Condens. Matter Phys. **1**:347369 (2010).
- [3] F. Bolton and D. Weaire, Phys. Rev. Lett. **65**, 3449 (1990).
- [4] D. J. Durian, Phys. Rev. Lett. **75**, 4780 (1995).
- [5] J. Brujić, S. F. Edwards, I. Hopkinson, and H. A. Makse, Physica A **327**, 201 (2003).
- [6] J. Zhou, S. Long, Q. Wang, and A. D. Dinsmore, Science **312**, 1631 (2006).
- [7] K. N. Nordstrom, E. Verneuil, P. E. Arratia, A. Basu, Z. Zhang, A. G. Yodh, J. P. Gollub, and D. J. Durian, Phys. Rev. Lett. **105**, 175701 (2010).
- [8] M. Mailman, C. F. Schreck, C. S. O'Hern and B. Chakraborty, Phys. Rev. Lett. **102**, 255501 (2009)
- [9] E. Lerner, G. Düring, and M. Wyart, Proc. Natl. Acad. Sci. USA **109**, 4798 (2012).
- [10] L. Cipelletti and L. Ramos, J. Phys.: Condens. Matter **17**, R253 (2005).
- [11] A. Ikeda, L. Berthier, and P. Sollich, Phys. Rev. Lett. **109**, 018301 (2012).
- [12] J. Seth, L. Mohan, C. Locatelli-Champagne, M. Cloitre, and R. Bonnecaze, Nature Materials **10**, 838 (2011).
- [13] S. Henkes, Y. Fily, and M. C. Marchetti, Phys. Rev. E **84**, 040301 (2011).
- [14] D. Bi, J. H. Lopez, J. M. Schwarz, and M. L. Manning, Nature Physics **11**, 1074-1079 (2015).
- [15] H. A. Makse, D. L. Johnson and L. M. Schwartz, Phys. Rev. Lett. **84**, 4160 (2000).
- [16] C. S. O'Hern, S. A. Langer, A. J. Liu, and S. R. Nagel, Phys. Rev. Lett. **88**, 075507 (2002).
- [17] L. E. Silbert, G. S. Grest, and J. W. Landry, Phys. Rev. E **66**, 061303 (2002).
- [18] C. S. O'Hern, L. E. Silbert, A. J. Liu, and S. R. Nagel, Phys. Rev. E **68**, 011306 (2003).
- [19] M. Wyart, S. R. Nagel, and T. A. Witten, Europhys. Lett. **72**, 486 (2005).
- [20] L. E. Silbert, A. J. Liu and S. R. Nagel, Phys. Rev. Lett. **95**, 098301 (2005).
- [21] S. Henkes, B. Chakraborty and C. S. O'Hern, Phys. Rev. Lett. **99**, 038002 (2007).
- [22] S. Henkes and B. Chakraborty, Phys. Rev. E **79**, 061301 (2009).
- [23] W. G. Ellenbroek, M. van Hecke, and W. van Saarloos, Phys. Rev. E **80**, 061307 (2009).
- [24] M. Wyart, S. R. Nagel, and T. A. Witten, Europhys. Lett. **72**, 486 (2005).
- [25] M. Wyart, Phys. Rev. Lett. **109**, 125502 (2012).
- [26] C. P. Goodrich, A. J. Liu, and J. P. Sethna, Proc. Natl. Acad. Sci. USA, **113** (35), 9673 (2016).
- [27] K. Ramola and B. Chakraborty, arXiv:1604.06148 (2016).
- [28] P. Olsson and S. Teitel, Phys. Rev. Lett. **99**, 178001 (2007).
- [29] W. G. Ellenbroek, E. Somfai, M. van Hecke and W. van Saarloos, Phys. Rev. Lett. **97** 258001 (2006).
- [30] C. P. Goodrich, A. J. Liu, and Sidney R. Nagel, Phys. Rev. Lett. **109**, 095704 (2012).
- [31] M. S. van Deen, J. Simon, Z. Zeravcic, S. D.-Bohy, B. P. Tighe and M. van Hecke, Phys. Rev. E, **90**, 020202(R) (2014).
- [32] R. Blumenfeld and S. F. Edwards, Eur. Phys. J. E **19**, 23 (2006).
- [33] R. Hihinashvili and R. Blumenfeld, Granular Matter **14**, 277 (2012).
- [34] T. Matsushima and R. Blumenfeld, Phys. Rev. Lett. **112**, 098003 (2014).

## Supplemental Material for “Scaling Theory for the Frictionless Unjamming Transition”

In this document we provide details of the calculations presented in the main text.

### Two point distribution $p(\vec{r}_1, \vec{r}_2)$

In this section we develop a diagrammatic expansion for the two point distributions of contact vectors  $p(\vec{r}_1, \vec{r}_2)$ . From Eq. (10) in the main text we have

$$p(\vec{r}_1, \vec{r}_2) = p(|\vec{r}_1|)p(|\vec{r}_2|)p(\theta). \quad (21)$$

along with

$$\int d^2\vec{r}_2 p(\vec{r}_1, \vec{r}_2) = p(\vec{r}_1) = \frac{1}{2\pi}p(|\vec{r}_1|), \quad (22)$$

where  $p(\vec{r}_1)$  represents the one point distribution of contact vectors. We then have

$$p(\theta) = \frac{p(\vec{r}_1, \vec{r}_2)}{p(|\vec{r}_1|)p(|\vec{r}_2|)} \quad (23)$$

This function  $p(\theta)$  therefore encodes the non-trivial correlations between the vectors that arise from the loop constraints mentioned in Eq. (7) in the main text. These constraints depend on the number of sides  $z_v$  within each cycle. In order to compute the above angular distribution, it is therefore useful to split the joint distribution of the vectors  $\vec{r}_1, \vec{r}_2$  into separate categories based on the minimum cycles to which they belong. We do this as follows

$$p(\vec{r}_1, \vec{r}_2) = \underbrace{3p(3)p(\vec{r}_1, \vec{r}_2|3)}_{p(\vec{r}_1, \vec{r}_2, 3)} + \underbrace{4p(4)p(\vec{r}_1, \vec{r}_2|4)}_{p(\vec{r}_1, \vec{r}_2, 4)} + \dots \quad (24)$$

where  $p(n)$  is the probability of occurrence of a minimum cycle with  $z_v = n$  sides,  $p(\vec{r}_1, \vec{r}_2|n)$  is the conditional probability that given a cycle with  $z_v = n$  sides two adjacent vectors are  $\vec{r}_1, \vec{r}_2$ ,  $p(\vec{r}_1, \vec{r}_2, n)$  represents the joint probability of occurrence of vectors  $\vec{r}_1, \vec{r}_2$  together with a cycle of  $z_v = n$  sides, and the combinatorial factor accounts for the different ways in which the vectors can be placed within the cycle.

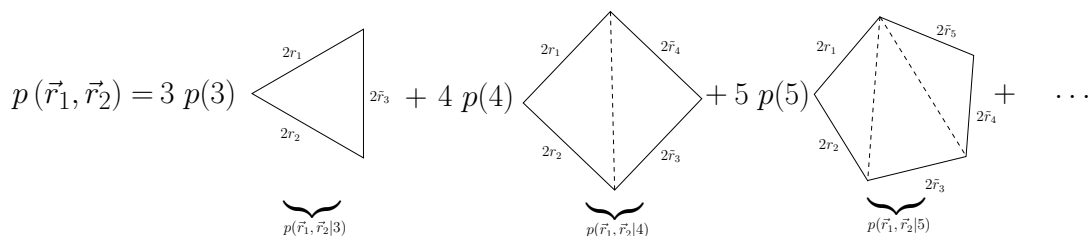


FIG. 4: Diagrams appearing in the expansion for the joint distribution  $p(\vec{r}_1, \vec{r}_2)$ . The different terms correspond to the minimum cycles with different numbers of sides. The vectors  $\vec{r}$  are integrated over. The terms corresponding to  $z_v = 3$  have a fixed length for all the sides and therefore give rise to angular distributions localized around a single value  $\theta = \arcsin \frac{\sqrt{3}}{2}$ . The terms corresponding to  $z_v > 3$  have unconstrained sides (depicted with dashed lines) and therefore contribute a finite amount to the angular distribution at  $\theta = \pi/2$ .

Next, the marginal distribution of these two vectors can be computed from the joint distribution of all the vectors in the cycle as

$$p(\vec{r}_1, \vec{r}_2|n) = \int_0^1 d\tilde{r}_3 \int_0^1 d\tilde{r}_4 \dots \int_0^1 d\tilde{r}_n p(\vec{r}_1, \vec{r}_2, \vec{r}_3, \vec{r}_4, \dots, \vec{r}_n|n), \quad (25)$$

where  $p(\vec{r}_1, \vec{r}_2, \vec{r}_3, \vec{r}_4, \dots, \vec{r}_n|n)$  represents the probability that a given minimum cycle of  $z_v = n$  sides has the (ordered) set of vectors  $\vec{r}_1, \vec{r}_2, \vec{r}_3, \vec{r}_4, \dots, \vec{r}_n$ . We represent this decomposition as a diagrammatic expansion in Fig 4.

In order to proceed further, we next make the crucial assumption that the joint probability of occurrence of the  $n$  vectors can be represented as a product form, along with the loop constraints. We have

$$p\left(\vec{r}_1, \vec{r}_2, \vec{r}_3, \vec{r}_4, \dots, \vec{r}_n | n\right) = p(\vec{r}_1)p(\vec{r}_2)p(\vec{r}_3)p(\vec{r}_4)\dots p(\vec{r}_n) \times \delta\left(\vec{r}_1 + \vec{r}_2 + \vec{r}_3 + \vec{r}_4 + \dots, \vec{r}_n\right), \quad (26)$$

where each  $p(r)$  is chosen from the one point distribution in Eq. (22). This somewhat drastic assumption is justified by the very good agreement between the angular and area distributions obtained from numerical simulations and those obtained by this analysis. This highlights the fact that the crucial correlations in the system arise primarily from these loop constraints. Finally, in order to simplify the analysis further, we assume that each of the contact vector lengths are drawn from a uniform distribution with width  $\sqrt{E_G}$ , consistent with the scaling form provided in Eq. (8) in the main text. We have

$$p\left(r = \frac{|\vec{r}|}{\sigma_g}\right) = \frac{1}{\sqrt{E_G}} \Theta\left(r - 1 + \sqrt{E_G}\right) \Theta(1 - r). \quad (27)$$

As the energy of the system approaches zero, the fluctuations in the lengths decrease and  $r \sim 1$ . From Fig. 4 it is clear that there is a fundamental difference between cycles with  $z_v = 3$  and  $z_v > 3$  sides. This is because the structures with  $z_v = 3$  have a fixed length for all the sides and therefore give rise to angular distributions localized around a single value  $\theta = \arcsin \frac{\sqrt{3}}{2}$ . We derive the angular distribution for the  $z_v = 3$  case using the above assumptions in the next section. The terms corresponding to  $z_v > 3$  have unconstrained sides (as depicted with dashed lines) and therefore contribute a finite amount to the angular distribution at  $\theta = \pi/2$ .

### Ordered Structures ( $z_v = 3$ )

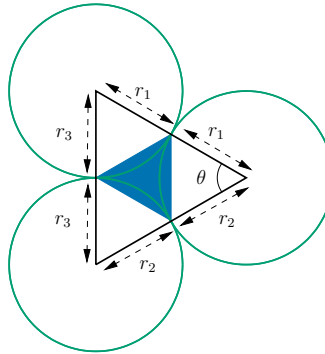


FIG. 5: The three-disk minimum cycle used to compute the angular distribution in Eq. (29) and the area distribution in Eq. (30). In our analysis we focus only on the case where all the disks have an equal size.

In this section, we compute the distribution of areas for the  $z_v = 3$  cycles and provide the scaling form for the “ordered divergence” mentioned in the main text. From Fig. 5 it is straightforward to compute

$$\sin \theta = \frac{\sqrt{4r_1^2 r_2^2 - (r_1^2 + r_2^2 - r_3^2)}}{2r_1 r_2}. \quad (28)$$

Using the product assumption in Eq. (26), the distribution of the angles for finite energies corresponding to the  $z_v = 3$  cycles can be computed as

$$p(\sin \theta, 3) = \int_0^1 dr_1 \int_0^1 dr_2 \int_0^1 dr_3 p(r_1)p(r_2)p(r_3) \delta\left(\sin \theta - \frac{\sqrt{4r_1^2 r_2^2 - (r_1^2 + r_2^2 - r_3^2)}}{2r_1 r_2}\right). \quad (29)$$

Similarly, the distribution of areas for the  $z_v = 3$  cycles can be computed as

$$p(\alpha, 3) = \int_0^1 dr_1 \int_0^1 dr_2 \int_0^1 dr_3 p(r_1)p(r_2)p(r_3) \delta\left(\alpha - \frac{\sqrt{4r_1^2 r_2^2 - (r_1^2 + r_2^2 - r_3^2)}}{4}\right). \quad (30)$$

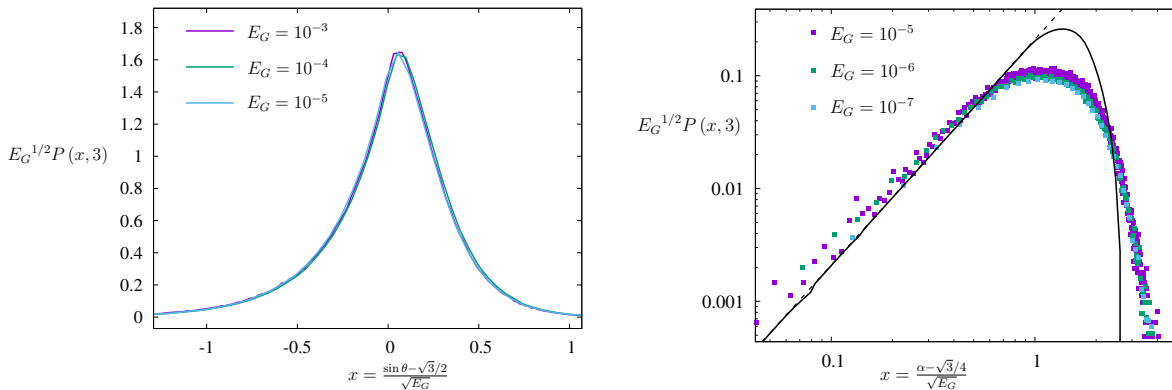


FIG. 6: **(Left)** Scaling collapse of the theoretical distribution of  $p(\sin \theta, 3)$  obtained by numerically integrating Eq. (29). The distribution obeys the scaling form provided in Eq. (31). **(Right)** Scaling collapse of the distribution of contact areas of the  $z_v = 3$  cycles obtained from numerical simulations along with the prediction from the theory. The plot shows the distribution of  $x = (\alpha - \sqrt{3}/4) / \sqrt{E_G}$ . The bold line represents the theoretical distribution obtained by numerically integrating Eq. (30) using a uniform distribution of contact vector lengths given in Eq. (27). The dashed line has a slope 2.

Replacing  $p(r)$  with the uniform distributions in Eq. (22) we find the following scaling form for the angular distribution

$$p(\sin \theta, 3) = \frac{1}{\sqrt{E_G}} \mathcal{P}_\theta \left( \frac{\sin \theta - \frac{\sqrt{3}}{2}}{\sqrt{E_G}} \right). \quad (31)$$

This behaviour is illustrated in Fig. 5 where we plot the angular distributions computed numerically using Eq. (29). Similarly, this leads to the following scaling form for the ordered divergence in the distribution of areas

$$p(\alpha, 3) = \frac{1}{\sqrt{E_G}} \mathcal{P}_O \left( \frac{\alpha - \frac{\sqrt{3}}{4}}{\sqrt{E_G}} \right), \quad (32)$$

which is Eq. (4) in the main text. This scaling behaviour is illustrated in Fig. 5 where we plot the distribution of areas computed numerically using Eq. (30), along with the distributions obtained from numerical simulations. We find a good agreement between the distributions in the limit  $\alpha \rightarrow \sqrt{3}/4$ . The scaling function has the following behaviour

$$\mathcal{P}_O(x) \sim x^2 \quad \text{for } x \rightarrow 0. \quad (33)$$

We note that in our analysis we have only focussed on monodispersed disks. The generalization to the polydisperse case involves all combinations of disks that can produce a  $z_v = 3$  cycle. For the bidispersed case with diameter ratio 1 : 1.4 that we simulate, the peaks in the area distribution occur at  $\alpha = \sqrt{3}/4 = 0.433013$  (for equal sized disks), 0.406116, 0.45453, 0.378775 and 0.473803 [27]. The scaling analysis for each of these cases remains the same.

#### Disordered Distribution: $p_{\text{DO}}(\alpha)$

In this section we derive an expression for the disordered divergence  $p_{\text{DO}}(\alpha)$  in the distribution of areas. We begin by assuming a product form for the joint distribution of contact vectors

$$p(\vec{r}_1, \vec{r}_2) = \frac{1}{2\pi} p(r_1) p(r_2). \quad (34)$$

In the above decomposition, we have assumed a uniform distribution for  $p(\theta)$  in the region  $[0, 2\pi]$ . This assumption is justified since we are interested in the distribution close to  $\theta \sim \pi/2$ . The analysis presented in this section can easily be generalized to smaller ranges of  $\theta$ . We have checked that the scaling features of the distribution near the transition are unchanged by extending the range of  $\theta$ . We then have

$$p(\sin \theta) = \frac{1}{2\pi} \frac{1}{\sqrt{1 - \sin^2 \theta}} \quad (35)$$

Next, from Eq. (9) in the main text we have the following equation for the distribution of the areas

$$p(\alpha) = \int_0^1 dr_1 \int_0^1 dr_2 \int_0^1 d\sin\theta p(r_1)p(r_2)p(\sin\theta) \delta\left(\frac{1}{2}r_1r_2\sin\theta - \alpha\right) \quad (36)$$

Once again to simplify the analysis, we replace the one point distribution of contact vector lengths  $p(r)$  by the uniform distribution in Eq. (27). Finally, performing the integral over  $\sin\theta$  we arrive at the following expression for the distribution of areas

$$p_{\text{DO}}(\alpha) = \frac{4}{\pi E_G} \int_{1-\sqrt{E_G}}^1 \int_{1-\sqrt{E_G}}^1 \frac{\Theta(xy - 2\alpha)}{\sqrt{x^2y^2 - 4\alpha^2}} dx dy. \quad (37)$$

In order to perform this computation we compute the simpler indefinite integral defined as

$$S_{\text{DO}}(\alpha, x, y) = \int \int \frac{1}{\sqrt{x^2y^2 - 4\alpha^2}} dx dy. \quad (38)$$

This does not explicitly contain the  $\Theta$  function. We can account for the  $\Theta(xy - 2\alpha)$  constraint by breaking the definite integral into regions depending on the value of  $\alpha$ . The definite integral can then be expressed as combinations of the above indefinite integral. We have

$$p_{\text{DO}}(\alpha) = \frac{4}{\pi E_G} \left( S_{\text{DO}}(\alpha, 1, 1) - S_{\text{DO}}(\alpha, 1, 1 - \sqrt{E_G}) - S_{\text{DO}}(\alpha, 1 - \sqrt{E_G}, 1) + S_{\text{DO}}(\alpha, 1 - \sqrt{E_G}, 1 - \sqrt{E_G}) \right). \quad (39)$$

#### Explicit expression for $S_{\text{DO}}(\alpha, x, y)$

We derive below an exact expression for the above indefinite integral  $S_{\text{DO}}(\alpha, x, y)$ . First, performing the integral over  $x$  we arrive at

$$S_{\text{DO}}(\alpha, y) = \int \frac{\log\left(y\sqrt{x^2y^2 - 4\alpha^2} + xy^2\right)}{y} dy \quad (40)$$

Next, the integral with respect to  $y$  can be performed exactly. After some algebraic simplifications (using Mathematica), the explicit expression is

$$\begin{aligned} S_{\text{DO}}(\alpha, x, y) = & -\frac{1}{2}\text{Li}_2\left(\frac{2\alpha^2}{2\alpha^2 - xy(xy + \sqrt{x^2y^2 - 4\alpha^2})}\right) - \frac{1}{2}\log^2\left(\sqrt{x^2y^2 - 4\alpha^2} + xy\right) + \log(xy)\log\left(\sqrt{x^2y^2 - 4\alpha^2} + xy\right) \\ & + \log(2)\log\left(\frac{\sqrt{x^2y^2 - 4\alpha^2}}{x} + y\right) + \frac{1}{2}\log(\alpha)\log\left(\frac{\alpha}{x^2}\right) + \frac{1}{2}\log^2(y) - \frac{\pi^2}{8} - \frac{1}{2}\log^2(2), \end{aligned} \quad (41)$$

where  $\text{Li}_2$  is the Polylogarithm function. Although the above expression is not explicitly symmetric under the  $(x, y) \rightarrow (y, x)$  transformation, it is easy to see that the expression  $p_{\text{DO}}(\alpha)$  preserves this symmetry. Using Eq. (41) it is straightforward to show (for example, using Mathematica) that the function  $p_{\text{DO}}(\alpha)$  given in Eq. (39) has the asymptotic behaviours mentioned in the scaling form in Eq. (3) in the main text.